Journal of
Materials Chemistry C

PAPER

View Article Online
View Journal

Cite this: DOI: 10.1039/c6tc00383d

Transparent conductive $CuCrO_2$ thin films deposited by pulsed injection metal organic chemical vapor deposition: up-scalable process technology for an improved transparency/conductivity trade-off

J. Crêpellière,*[a] P. Lunca Popa,[a] N. Bahlawane,[a] R. Leturcq,[a] F. Werner,[b] S. Siebentritt[b] and D. Lenoble*[a]

Received 26th January 2016,
Accepted 25th March 2016

DOI: 10.1039/c6tc00383d

www.rsc.org/MaterialsC

Metal organic chemical vapor deposition is carefully optimized for the growth of pure $CuCrO_2$ delafossite coatings on glass substrates. The pulsed direct liquid delivery is demonstrated to be an efficient process technology for the controlled supply of the precursor solution in the evaporation chamber, which is shown to be one of the main process parameters to tailor the thin-film properties. We investigated the influence of the precursor concentration ratio $Cu(thd)_2$ (bis[2,2,6,6-tetramethyl-3,5-heptanedionato]copper(II)) and $Cr(thd)_3$ (tris[2,2,6,6-tetramethyl-3,5-heptanedionato]chromium(III)) on the crystal structure, morphology and electrical conductivity, at a reduced temperature of 370 °C. We observe for a low ratio, a pure delafossite phase with a constant Cu-poor/Cr-rich chemical composition, while at a high ratio a mixture of copper oxides and $CuCrO_2$ was found. The as-grown 140 nm-thick pure delafossite films exhibit an exceptional high electrical conductivity for a non-intentionally doped $CuCrO_2$, 17 S cm^{-1}, and a near 50% transparency in the visible spectral range.

Introduction

Electrical conductivity and optical transparency are antagonistic properties of materials as the band structure requirements contrast significantly. While for a good transparency, a wide band gap (>3 eV) is necessary in order to avoid light absorption, semiconductor materials are characterized by a narrow band gap (<2 eV) and low activation energy of charge carriers to tune their electrical conductivity at room temperature. The very first reported transparent conducting material (TCM) was cadmium oxide CdO back in 1952.[1] It belongs to the transparent conductive oxide (TCO) class, an important sub-category of TCMs. TCOs have initially wide band gaps and are subsequently extrinsically doped in order to modify the charge carrier concentration without altering the optical properties.[2,3]

Nowadays TCOs are widely used in different technology fields such as transparent electrodes in flat panel displays, light-emitting diodes, solar cells and touch panels.[4–8] The most used TCOs are Sn-doped In_2O_3 (ITO),[9] SnO_2[10] or ZnO,[11] which feature n-type conductivity. However, the development of modern electronic circuitry or optoelectronic devices is based on p–n junctions, and therefore needs also the use of p-type materials.[12] Although n-type materials with high conductivity and transparency were demonstrated,[2] p-type TCOs still need an archetypal material. Some of the most promising p-type materials are delafossite compounds AMO_2 (with A = Cu or Ag and M = Al, Sc, Cr, Fe, Ga, or Y),[13] which have been thoroughly studied for more than twenty years. Kawazoe *et al.* proposed a model of chemical modulation of the valence band, in order to explain the high mobility measured for $CuAlO_2$ (>1 cm^2 V^{-1} s^{-1}).[14,15] To date, the highest reported conductivity of delafossite was 220 S cm^{-1} for Mg doped $CuCrO_2$.[16] One can however notice that this result was not reproduced or confirmed by other research groups. Copper chromium oxides contrast with other delafossites, in terms of: (i) high density of state of 3d M cations (Cr^{3+}) near the valence band maximum, (ii) covalent mixing between chromium and oxygen ions and (iii) good dopability,[17–22] making $CuCrO_2$ a good p-type candidate for transparent electronic devices.

Several methods were reported in the literature for the synthesis of $CuCrO_2$: solid-state reaction (SS),[17,20–30] sol–gel (SG),[31–37] pulsed laser deposition (PLD),[38–42] magnetron

[a] Material Research and Technology Department, Luxembourg Institute of Science and Technology, 5 Avenue des Hauts-Fourneaux, L-4362 Esch-sur-Alzette, Luxembourg. E-mail: jonathan.crepelliere@list.lu, damien.lenoble@list.lu
[b] Laboratory for Photovoltaics, Physics and Materials Science Research Unit, University of Luxembourg, Luxembourg

Table 1 Summary of $CuCrO_2$ synthesis methods

	Growth		Annealing				
Synthesis	Temperature (°C)	Time (h)	Temperature (°C)	Time (h)	σ (S cm^{-1})	Transmission (%)	Thickness (nm)
SS	850–1200	12–48	900–1200	10–100	10^{-4}–10^{-3}	Not reported	Not reported
SG	300–500	0.1–1	700–800	0.5–2	6.10^{-4}–10^{-2}	45–60	100–200
PLD	550–750	0.5–2	None	None	1–5	55–65	60–130
MS	RT	1	600–900	2–4	10^{-3}–1	40–60	100–300
	750	1.5	None	None			
CVD	240–550	0.5	700–950	Not reported	1–2	40	400
Spray pyr.	345	1	None	None	12	55	70

sputtering (MS)[16,43–46] and chemical vapor deposition (CVD) including spray pyrolysis.[47–50] A summary of the electrical and optical properties *versus* the synthesis methods and the process temperature is given in Table 1. The most intensively reported $CuCrO_2$ synthesis method is the solid-state method. The $CuCrO_2$ SS synthesis consists of mixing and grinding Cu_2O and Cr_2O_3 powders before sintering at 850–1200 °C in air or a nitrogen atmosphere for 12–48 hours. Additional steps of regrinding and calcination of the mixture can be necessary, at 900–1200 °C for 10–100 h to achieve good crystalline quality. The SS synthesis method is still essentially used to provide model materials for fundamental studies related to electronic structures,[17] carrier transport mechanisms,[20] magnetic,[27–29] thermoelectric[23,24] and photocatalytic[25] investigations. Sol–gel is another well reported synthesis method of $CuCrO_2$. Copper and chromium hydrate precursors are dissolved in alcoholic solution and then deposited by spin coating on quartz or sapphire substrates. After drying between 300 and 500 °C for 5–60 min, deposition and drying are repeated until the desired thickness is reached. Annealing at 700–800 °C under a pure nitrogen atmosphere is necessary to obtain films with a pure delafossite structure. Suitable transparency (55% in visible range) but relative poor conductivities ($\approx 10^{-4}$–10^{-2} S cm^{-1}) are obtained with the films deposited by sol–gel, due to the low carrier concentration. The required high processing temperatures exclude the direct involvement of SS and SG for the fabrication of transparent electronic devices on transparent substrates like glass or plastic. However, SS and SG are useful for the synthesis of targets for the PLD and MS methods. The PLD of chromium copper oxide films was reported at 450–750 °C, but crystalline delafossite $CuCrO_2$ is only observed for temperature higher than 550 °C. Two approaches were reported using MS for the synthesis of delafossite $CuCrO_2$. In a first approach, the deposition is performed at low temperature followed by annealing at high temperature, 600–900 °C, or the deposition is performed directly at high temperature, 750 °C. The optical transparency of films obtained using these processes is comparable to the films obtained by sol–gel, but electrical conductivity is enhanced by a factor of up of 100 to reach typically 0.1–1 S cm^{-1}. As for sol–gel and solid-state reactions, the involved synthesis temperatures in the PLD and MS processes are still higher than 500 °C and make the use of such techniques hardly compatible with the manufacturing requirements of active transparent electronic devices. Chemical vapor deposition (CVD) synthesis was also used to grow $CuCrO_2$. Amorphous films, or delafossite $CuCrO_2$ contaminated with the spinel $CuCr_2O_4$ phase, were reported at processing temperatures between 240 and 550 °C.[47,51] Annealing under an argon atmosphere at 700–950 °C was used to crystallize $CuCrO_2$ or to convert the spinel phase into a delafossite one.[47,51] To our knowledge, no synthesis method, which is compatible with the manufacturing requirements, was reported, until very recently, to produce at low cost (one step process) pure delafossite $CuCrO_2$ thin-films at moderate temperatures (below 400 °C) over a large substrate area. Our group disclosed during the fifth international symposium on transparent conductive materials in 2014 the use of metal–organic chemical vapour deposition to grow $CuCrO_2$ thin-films at low temperature (<500 °C).[52] More recently, Farrell *et al.*[49] reported the growth of Cu_xCrO_y at low temperature ($\approx$345 °C) by spray pyrolysis. However, they reported XRD diffraction peaks (2θ = 36.4°) that can also be attributed to copper or chromium oxide phases. The characteristic peaks of polycrystalline $CuCrO_2$ at 2θ = 31.1° and 2θ = 40.9° as reported by Barnabé *et al.* are missing, and the 1 : 2 : 4 ratio of Cu : Cr : O in films raises doubts about the exclusive presence of the $CuCrO_2$ phase in films. Moreover, the lack of a significant increase of absorption coefficient for photon energy higher than 3 eV is surprising for $CuCrO_2$ materials having a direct bandgap >3 eV. In a very recent paper of the *Journal of Materials Chemistry C*,[53] Farrell *et al.* further investigated the synthesis of nanocrytalline Cu deficient Cu_xCrO_y phases confirming Cu-deficiency and O-rich stoichiometry of the grown films with an optimum stoichiometry of $Cu_{0.4}CrO_{2.5}$ or $Cu_{0.8}Cr_2O_5$. Good conductivity and transparency tradeoff were disclosed for such thin films grown with Cu(acac)$_2$ (bis[2,4-pentanedionato]copper(II)) and Cr(acac)$_3$ (tris[2,4-pentanedionato]chromium(III)) precursors.

In the present paper we report, for the first time, the growth of nominally undoped chromium copper delafossite thin films using direct liquid injection chemical vapor deposition. The main process parameters like the growth temperature and the composition of the precursor solution are optimized. The crystalline properties, morphology and chemistry of the thin films are thoroughly studied together with the electrical and optical properties. Electrical analysis includes the first successful measurements of the experimental Hall mobility of delafossite Cu_xCrO_2 using a high magnetic field setup (9 T). The interplay between the thin-film properties and the electrical/optical trade-off is investigated demonstrating the benefits of the MOCVD process for the synthesis of delafossite phases of Cu_xCrO_2 thin-films.

Experimental methods

Thin films were deposited using pulsed injection MOCVD, (MC200, Annealsys), which is a stagnation point-flow warm-wall reactor. The used copper and chromium precursors are bis[2,2,6,6-tetramethyl-3,5-heptanedionato]copper(II) and tris[2,2,6,6-tetramethyl-3,5-heptanedionato]chromium(III), respectively ($Cu(thd)_2$ and $Cr(thd)_3$, Strem Chemicals). Cyclohexane solutions with a total precursor concentration of $[Cu(thd)_2] + [Cr(thd)_3] = 5$ mM and adjusted $Cu(thd)_2$ mole fraction $\chi = [Cu(thd)_2]/([Cu(thd)_2] + [Cr(thd)_3])$ were prepared. The mole fraction was varied from 0 to 1. The precursor is then maintained under a nitrogen pressure of 5 bars at room temperature before its injection into the evaporation chamber with a frequency of 5 Hz and a feeding rate of 0.8 g min^{-1}. The pressure and temperature of the evaporation chamber were maintained at 6 mbar and 225 °C during deposition. The walls of the reactor were maintained at 225 °C and the oxidation of the precursors during the growth was ensured by molecular oxygen. The flow rate of oxygen was set at 800 sccm (standard cubic centimeter per minute) with a nitrogen flow rate of 2050 sccm. The temperature of the substrate surface was varied within the 330–430 °C range and was measured using *in situ* thermocouples (K-type).

Prior to the deposition process, the glass substrates were ultrasonically cleaned in ethanol, and acetone, dried with a nitrogen jet and then exposed for 15 minutes to oxygen plasma generated *in situ* the chamber.

The structure of the grown films was studied by X-Ray Diffraction (XRD), Bruker D8 Discover, using monochromatic Cu Kα radiation (λ = 1.54 Å) at 40 kV and 40 mA. The analyses were performed using the Grazing Incidence (0.5°) X-Ray Diffraction (GIXRD) at a scanning step of 0.02°.

X-Ray Photoemission Spectroscopy (XPS) was performed using a Kratos Axis Ultra DLD system using a monochromated (Al Kα: $h\nu$ = 1486.7 eV) X-ray source. The surface morphology of the films was inspected by Scanning Electron Microscopy (SEM), FEI Helios 50 High Resolution. Electrical properties were measured using a four probe van der Pauw configuration at room temperature and at low temperature using a closed-cycle helium cryostat. Transport properties were determined, at room temperature, by Hall effect measurements using a DRYICEVTI Cryogen Free Top Loading 9T System from ICEoxford Ltd, and thermoelectric measurements were performed to extract the Seebeck coefficient. A Perkin Elmer Lambda 950 UV/Vis spectrometer was used to determine optical properties.

The absorption coefficient was calculated by assuming a non-coherent film with multiple reflection inside the thin-film and a non-absorbing substrate. Thus, the experimental reflection R and experimental transmission T are defined as:[54]

$$T = \frac{(1-r)^2 e^{-\alpha d}}{1 - r^2 e^{-2\alpha d}} \quad (1)$$

$$R = r + \frac{(1-r)^2 r e^{-2\alpha d}}{1 - r^2 e^{-2\alpha d}} \quad (2)$$

where r is the reflectance of a simple air/film interface, α is the absorption coefficient and d is the thickness of the film. If we consider a well absorbing film, only the first reflection is significant and:

$$r = R \quad (3)$$

$$T = (1 - r)^2 e^{-\alpha d} \quad (4)$$

By combining (3) and (4) the absorption coefficient becomes:

$$\alpha = \frac{1}{d}\ln\left(\frac{(1-R)^2}{T}\right) \quad (5)$$

Usually eqn (5) is used when absorption is high and multiple reflections inside the films can be neglected. In our case, we preferably consider multiple reflections into our thin-films. Therefore, eqn (1) and (2) are two equations with two unknown parameters (r and α) that can be resolved mathematically. Thus, the absorption coefficient is exactly defined by:

$$\alpha = \frac{1}{d}\ln\left(\frac{1}{2\sqrt{\frac{-p}{3}}\cos\left(\frac{1}{3}\arccos\left(\frac{-q}{2}\sqrt{\frac{27}{-p^3}}\right)\right) - \frac{b}{3a}}\right) \quad (6)$$

where

$$p = -\frac{b^2}{3a^2} + \frac{c}{a}$$

$$q = \frac{b}{27a}\left(\frac{2b^2}{a^2} - \frac{9c}{a}\right) + \frac{d}{a}$$

$$a = T^2$$

$$b = \left(2T - 2RT - T^3 + TR^2\right)$$

$$c = (1-R)^2 - 2T^2$$

$$d = -T$$

Such a model for α has been applied for our study.

Results and discussion

Crystalline structure

The effect of the deposition temperature on the crystallographic phases of the films was investigated using a precursor solution with χ = 0.33. The obtained diffractograms are displayed in Fig. 1(a). According to the International Center for Diffraction Data (ICDD) (pdf no. 04-010-3330), films obtained at $T_{surface}$ = 370 °C and $T_{surface}$ = 330 °C present a pure rhombohedral delafossite structure belonging to the $R3m$ space group. The evaluation of the relative intensity of the diffracted peaks shows a clear (012) preferential orientation (2θ = 36.4°) in the GIXRD configuration adopted, with an increasing (006) peak intensity (2θ = 31.5°) for deposition temperatures above 370 °C. Films deposited at $T_{surface}$ = 430 °C are characterized by the presence of Cu_2O and CuO phases (arrows in Fig. 1(a)). It is worth noticing that a pure delafossite structure is grown at

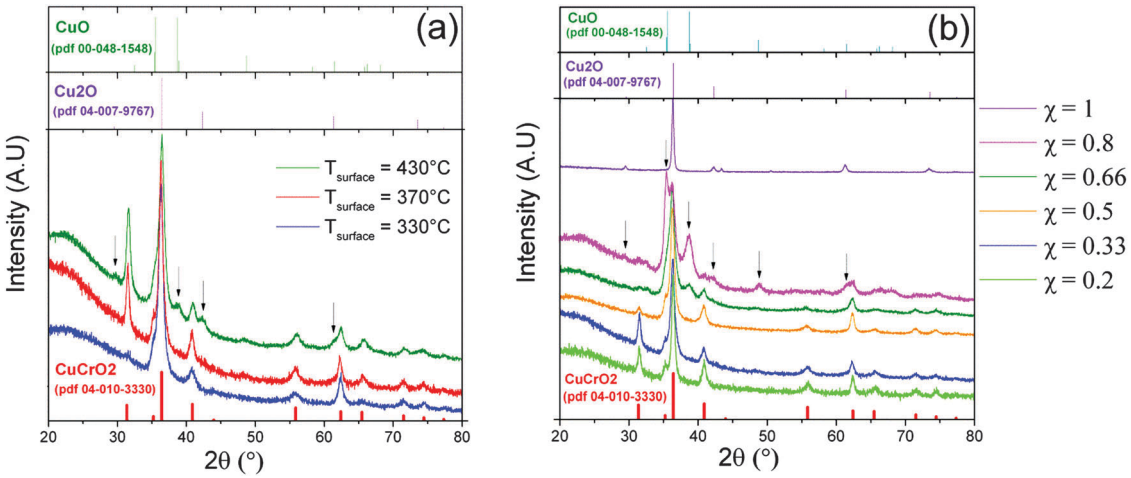

Fig. 1 (a) XRD diffractograms of films deposited at various substrate temperatures, $T_{surface}$ (330–430 °C), and using a precursor solution with χ = 0.33. The film thickness is between 120 and 160 nm. Bottom and top diagrams represent the expected peaks for the corresponding phases, according to the ICDD cards given in the figure. (b) Influence of the precursor composition on the crystallographic structure of the obtained films at $T_{surface}$ = 370 °C. Bottom and top diagrams represent the expected peaks for the corresponding phases, according to the ICDD cards given in the figure.

low temperature, $T_{surface}$ = 330 °C, and without any additional annealing step.

The impact of the $Cu(thd)_2$ mole fraction in the liquid precursor (χ) was investigated at the temperature of $T_{surface}$ = 370 °C, temperature that promotes the growth of a pure polycrystalline delafossite phase at χ = 0.33. The XRD diffractograms of films deposited at various values of χ are depicted in Fig. 1(b). Pure delafossite thin films are grown for $0.2 \leq \chi \leq 0.6$, while CuO and Cu_2O phases are evidenced for $\chi \geq 0.66$ (arrows in Fig. 1(b)). The Cu_2O phase is detected when deposition was carried out with a precursor solution featuring χ = 1, with a small signature of Cu metal at $2\theta = 43.5°$. It is worth nothing that no film is grown at χ = 0 (*i.e.* when pure $Cr(thd)_3$ is used) and that an excess of chromium precursor in the precursor solution does not lead to chromium oxide phases. Thus, deposition temperatures below 430 °C and with copper fraction $\chi < 0.66$ are necessary to avoid the formation of parasitic crystalline phases such as CuO and Cu_2O.

For pure delafossite thin films, the extracted lattice parameter c along the (006) direction, from the XRD results, is between 17.05 and 17.06 Å (±0.02 Å). It is slightly below the reported values at 17.10 Å for the rhombohedral delafossite structure of $CuCrO_2$.[55,56] The extracted parameter a, along the (012) direction (parameter *c* is known thanks to the (006) direction), is 2.98 ± 0.02 Å and is in good agreement with the values reported for crystalline $CuCrO_2$ delafossite (2.97 Å).[23,55,56] According to the crystalline parameters *a* and *c*, our materials lattice seems to be slightly compressed along the *c* axis by 0.3%. A pure polycrystalline delafossite $CuCrO_2$ phase is grown with large process windows of precursor ratio and temperature. This further reinforces the suitability of our pulsed-injection-CVD process for growing $CuCrO_2$ coatings over a large area.

Morphology

The surface SEM inspection (Fig. 2) indicates that the morphology of the pure phase delafossite is strongly influenced by the relative

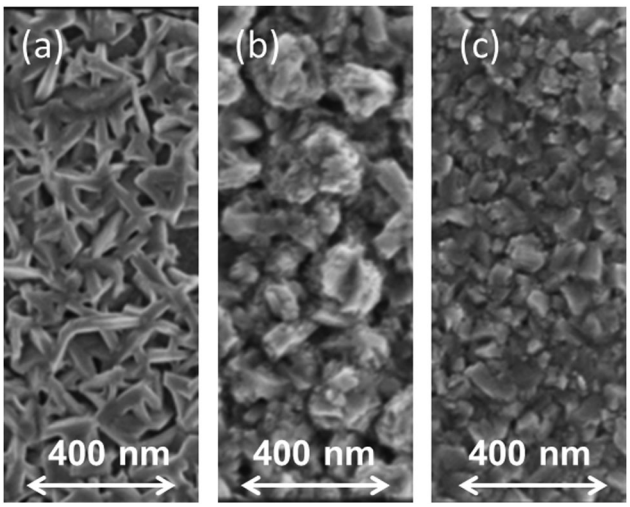

Fig. 2 Top view SEM micrographs for films deposited at $T_{surface}$ = 370 °C and (a) χ = 0.2, (b) χ = 0.33 and (c) χ = 0.6.

ratio of precursors in the solution χ. For χ = 0.2, the as-deposited films present a "spine" morphology, while for χ = 0.33 and χ = 0.6, a grainy structure is observed. Films are more compact and the grain size, as observed in SEM pictures, decreases when the ratio χ increases. As measured from the SEM pictures, the average grain size is (160 ± 60) nm for χ = 0.33, while (56 ± 27) nm is determined for χ = 0.6. The thin-film thicknesses measured from cross-sectional SEM observations are 120, 140 and 160 nm for χ = 0.2, 0.33 and 0.6, respectively. A continuous closely packed thin film is obtained for a Cu-rich precursor solution (χ = 0.6).

Yield synthesis of $CuCrO_2$ was determined for χ = 0.5 thin film, deposited on 1 $inch^2$ (6.25 cm^2) of the glass substrate. In that case, 268 mg and 376 mg of $Cu(thd)_2$ and $Cr(thd)_2$, respectively, were dissolved in 500 mL of cyclohexane. For a time deposition of 240 min, we measured a weight thin film

deposition (W_d) of 520 μg on glass while theoretical weight (W_{th}) must be 1.57 mg (W_{th} = 330 mg for a surface of 8'' wafers) Then, yield synthesis for χ = 0.5 is 33%.

XPS analysis

Chemical composition of the grown films on glass substrates was studied by *ex situ* XPS analysis and is given in Fig. 3(a). For pure delafossite films ($0.2 \leq \chi \leq 0.6$), an over-stoichiometric concentration of chromium is measured in the films even for $\chi > 0.5$ corresponding to a Cu-rich solution of precursors. It is reminded that no specific crystalline phase of chromium compound (except $CuCrO_2$) is detected by XRD in these cases. For $\chi > 0.66$, an excess of copper concentration is evident and is well in line with the concomitant detection of copper oxide phases. The graph inset in Fig. 3(a) shows the percentage of copper and chromium in films with pure phase delafossite for the different precursor ratios investigated in our study (with an error of 2%). It appears that the relative deficiency of copper in the films is mainly counter balanced by an excess of chromium in $CuCrO_2$ thin-films. The oxygen concentration close to the stoichiometric value of 50% is also a specific feature of our thin-films when compared to the optimized thin-films reported by Farrell *et al.*[53] (Suggesting in their case an excess of oxygen for the optimum stoichiometry of $Cu_{0.4}CrO_{2.5}$.)

Considering the chemical composition (Fig. 3(a)) and the growth rate (Fig. 3(b)) of our films *versus* the ratio of precursors, thin-films are grown only when the Cu precursor is present. As previously stated, a precursor solution of pure $Cr(thd)_3$ does not lead to any film growth under the process conditions that have been investigated in our study. Interestingly, the growth rate increases almost linearly from 0 to 1 nm min^{-1} when the Cu concentration is incrementally increased from χ = 0 to χ = 1. Moreover, in the range where only a $CuCrO_2$ polycrystalline phase is evidenced by XRD, the chemical concentration of Cr is almost stable while the growth rate is definitely increasing. We assume that the Cu precursor or Cu-byproducts catalyze the thermal decomposition of $Cr(thd)_3$ and the growth reaction of Cr with Cu and oxygen to grow $CuCrO_2$. We investigate the chemical environment of Cu and Cr in our pure $CuCrO_2$ delafossite thin films by detailed analysis of the XPS spectra. The XPS spectra of the deposited film with χ = 0.5 are shown in Fig. 4(a) before (top surface analysis) and after surface cleaning with the use of *in situ* argon ion beam (inside thin-film analysis chamber). While a C 1s peak is observed for the top-surface analysis of our thin-films, no carbon is detected anymore after the surface cleaning. Top-surface carbon contaminations are attributed to the exposure of our samples to the ambient air and correspond to organic residues on the sample surface. Carbon concentration in our thin-films is below 1 at%, (detection limit of the XPS analysis) highlighting the efficient surface reaction of our metal organic precursors and the fast removal of the carbonated by-products.

Cu 2p spectra after sputtering for films deposited with various ratios ($0.20 \leq \chi \leq 1.0$) are depicted in Fig. 4(b). All spectra are normalized to the Cu $2p_{3/2}$ peak. The XPS spectrum shows Cu $2p_{1/2}$ at (952.4 ± 0.1) eV and Cu $2p_{3/2}$ at (932.5 ± 0.1) eV, providing a spin orbit splitting energy in good agreement with the reported data in the literature for $CuCrO_2$ phases, *i.e.* $\Delta_{Cu\ 2p}$ = 19.9 ± 0.2 eV[57] for all ratios χ. One may remember that the determination of the oxidation state of Cu based on the fine analysis of Cu 2p is almost impossible when considering Cu^0 and Cu^{I+} oxidation states, because the two peaks are too closer. We also observed, for χ = 0.8, features at 944.0 eV and 940.8 eV (arrow in Fig. 4(b)), and a Cu $2p_{3/2}$ peak broader in the high energy range. These features indicate the presence of Cu^{II+} [58] for χ = 0.8, as confirmed by XRD analysis highlighting the CuO phase. Cr 2p XPS spectra after sputtering of $0.2 \leq \chi \leq 0.6$ are depicted in Fig. 5(a). All films exhibit Cr $2p_{1/2}$ and Cr $2p_{3/2}$ peaks at the same binding energies, *i.e.* 582.2 eV ± 0.1 eV and 576.6 ± 0.1 eV, respectively, which correspond to the (+III) oxidation state of Cr.[57] Interestingly, in the same range of energies, the Cu Auger peak (Cu LMM) is detected. The Cu LMM peak is centered at 569.9 ± 0.2 eV when the delafossite phase is contaminated by the presence of copper oxide phases ($0.66 \leq \chi \leq 1$), while the Cu LMM peak is 568.8 ± 0.1 eV, for the pure delafossite phase ($\chi < 0.66$). The reference spectra of CuO (Cu^{II+}), Cu_2O (Cu^{I+}) and Cu (Cu^0) were also measured on the same instrument and using the same protocol. The reference peaks of Cu are used for comparison of the Cu LMM

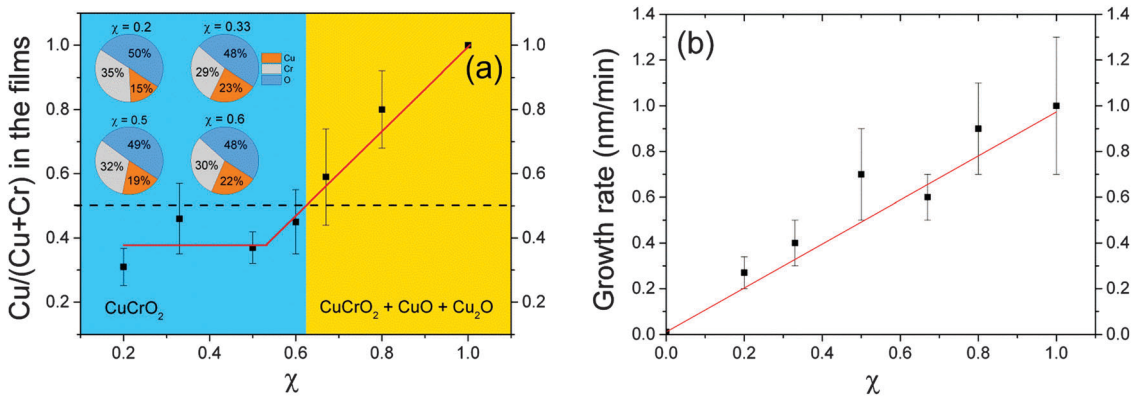

Fig. 3 (a) Chemical composition of film growth at 370 °C with precursor solutions featuring $0.2 \leq \chi_{Cu} \leq 0.8$ as measured using XPS. (b) Growth rate at $T_{surface}$ = 370 °C with precursor solutions featuring $0 \leq \chi \leq 1$, calculated from the film thickness measured from cross-sectional SEM images.

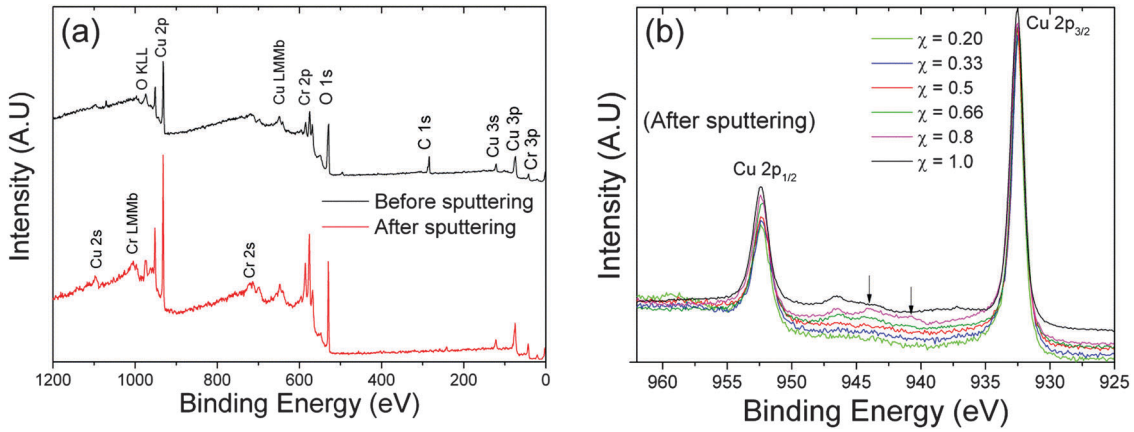

Fig. 4 (a) XPS spectrum, before and after surface cleaning, of the chromium copper oxide films grown with x_{Cu} = 0.5 and at temperature $T_{surface}$ = 370 °C. (b) High resolution Cu 2p XPS scans for films grown at $T_{surface}$ = 370 °C with $0.2 \leq \chi \leq 0.6$.

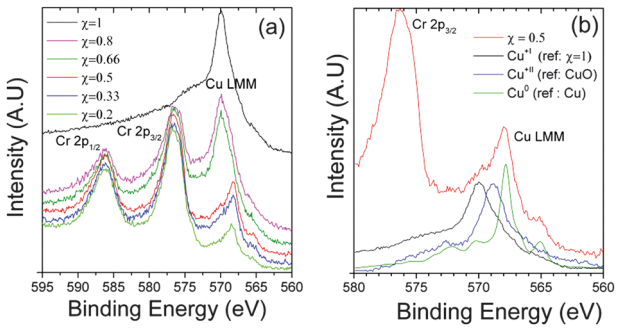

Fig. 5 (a) High resolution Cr 2p and Cu LMM XPS scans for films grown at $T_{surface}$ = 370 °C with $0.2 \leq x_{Cu} \leq 0.8$. (b) Cu LMM peak for χ = 0.5 and Cu LMM peaks of copper oxidation state Cu^0, Cu^{I+} and Cu^{II+}.

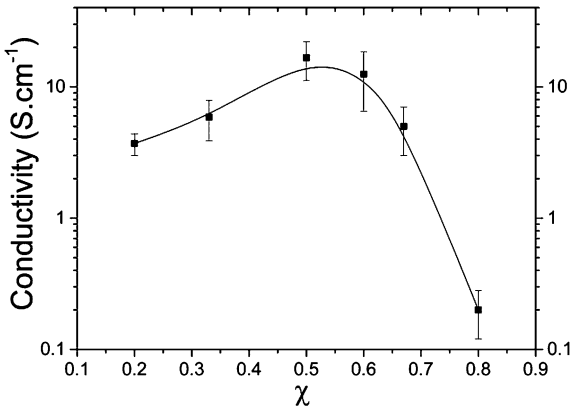

Fig. 6 Conductivity, measured in the van-der-Pauw configuration, as a function of the copper fraction χ in the precursors' solution for films grown at 370 °C.

peak obtained in the case of the pure delafossite phase (as shown by the XRD measurements) *i.e.* χ = 0.5. As depicted in Fig. 5(b), the Cu LMM peak is mainly due to the contribution of two oxidation states of copper, namely Cu^0 and Cu^{I+}. The Auger peak clearly highlights the presence of Cu^0 in our thin-films, however the determination of the respective concentration of Cu^0 and Cu^{I+} by the deconvolution of the Auger peak would lead to uncertain results and conclusions.

Interestingly, Arnold *et al.*[17] analyzed the Cu LMM peak (with Cr 2p peaks) of stoichiometric $CuCrO_2$, and they observed only a Cu^{I+} contribution. Knowing that our delafossite $CuCrO_2$ thin-films are Cr-rich (Cu: 20 ± 2% and Cr: 30 ± 2%), we may attribute our specific Cu LMM signature of Cu^0 to the influence of the excess of Cr (~+5%) which shall impact the chemical electronic environment of Cu atoms. A similar signature of the Cu LMM peak has been measured but not discussed by Farrell *et al.*,[49] who demonstrated the growth of Cr-rich Cu_xCrO_y using the spray pyrolysis process. The latter process seems to also induce the presence of Cu^0 in the films as-evidenced by the Cu LMM peak at 565 eV.

Electrical properties

Electrical conductivity at room temperature is plotted as a function of χ (Fig. 6) for a process temperature of $T_{surface}$ = 370 °C. For all samples, the thickness ranges from 120–160 nm. The highest conductivity, at 17 S cm^{-1}, was obtained for χ = 0.5, this conductivity is higher than published data (Table 1).

The observed morphology (Fig. 2) provides critical insights into the increase of the conductivity in the $\chi \leq 0.5$ range. Increasing the fraction of copper decreases the porosity of the thin-film morphology. In the range $\chi > 0.6$, the degraded conductivity is attributed to the incremental increase of the Cu_2O and CuO phases in the thin-films.

For the thin-film grown at 370 °C with χ = 0.5, Hall effect measurements were performed by varying the magnetic field between −9 and 9 T at a constant current of 0.25 mA. This led to a hole concentration of (9 ± 3) × 10^{21} cm^{-3} and a hole mobility μ_h of (1.1 ± 0.4) × 10^{-2} cm^2 $V^{-1}s^{-1}$. Such a measurement at a high magnetic field is mandatory to investigate the mobility of degenerated oxide semiconductors with low mobility.[59] It is worth highlighting that such a successful measurement has been reported for the first time for $CuCrO_2$ polycrystalline thin-films.

Thermopower measurements showed that the Seebeck coefficient was +110 μV K^{-1} for $CuCrO_2$ (x = 0.5) with metallic copper used as the reference electrode, and the p-type character

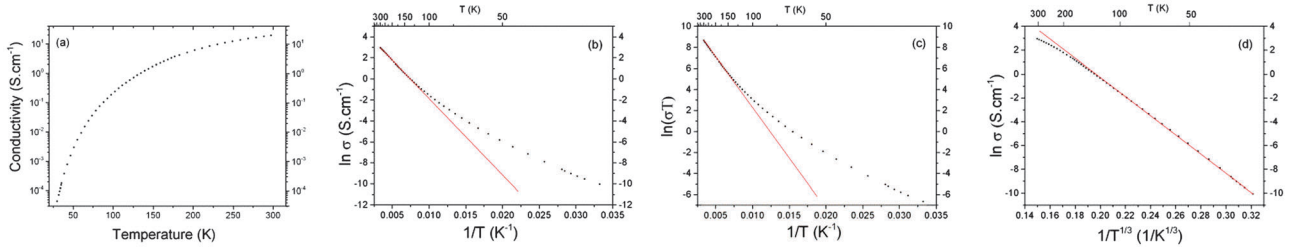

Fig. 7 (a) Conductivity of χ = 0.5 as a function of the temperature, (b) band conduction model, (c) small-polaron model and (d) VRH model with n = 2.

of our $CuCrO_2$ thin-films is evidenced and confirmed together with the Hall effect measurements. The Seebeck coefficient falls in the same range as the one reported by Barnabé *et al.*, while the conductivity reaches 17 S cm^{-1} for the thin-films grown for x = 0.5, similar to the one obtained by Farrell *et al.*[53]

The electrical conductivity as measured in the van-der-Pauw configuration continuously increases with the temperature increasing from 30 to 300 K (Fig. 7(a)), confirming the semiconducting behaviour of our thin-films. The electrical conductivity *versus* temperature between 150 and 300 K may be fitted by a classical thermally activated law (Fig. 7(b)) (if the band conduction model of classical semiconductors is used). The conductivity is expressed as:

$$\sigma = \sigma_0 e^{-\frac{E_a}{k_B T}} \quad (7)$$

where σ_0 is a pre-exponential factor (we consider that σ_0 is not temperature dependent), E_a is the activation energy, T is the temperature and k_B is the Boltzmann constant. The extracted transport activation energy is 63 meV, lower than $3k_BT$ at room temperature, leading thus to consider a strongly doped degenerated semiconductor behaviour with a significant population of acceptor levels close to the top of the valence band. The activation energy of transport is very well in line with the data reported by Barnabé *et al.*,[60] using a similar model of classical semiconductors (7).

However, considering the low mobility value as given by the Hall effect measurement and the relatively "high" effective mass of holes, m_{eff}, in $CuCrO_2$ (ranging from 4.5 to 6 units of free electron mass),[19] the mean free path λ of holes (in classical semiconductors) can be obtained by $\lambda = \nu_{th}\tau$ with ν_{th} being the thermal velocity of carriers at room temperature and τ being the mean free time of carriers (holes) between collisions. ν_{th} is defined by eqn (8), assuming a free hole with only kinetic energy:[61]

$$\nu_{th} = \sqrt{\frac{3k_B T}{m_{eff}}} \quad (8)$$

and τ is given by:

$$\tau = \frac{m_{eff}\mu_h}{q} \quad (9)$$

(q being the elementary charge).

λ ranges from 1.6–1.8.10^{-3} nm, indicating that the free hole model from the Drude approach[61] is not appropriate. It was consistently proposed that delafossite compounds exhibit electrical transport limited by small polaron hopping.[62,63] In this model, the carrier is strongly localized within the lattice potential. The coupling of the carrier with the lattice phonon forms polarons that are self-trapped. From a mechanistic point of view, Bosman and van Daal set the condition occurrence of self-trapping (small polaron model) as:[64]

$$\tau \gg \tau_0 \quad (10)$$

where τ is the time for the hole transition from ion to ion, and τ_0 is the time of a lattice vibration. The time τ can be calculated by:[64]

$$\tau = \frac{e a^2}{2\mu k_B T} \quad (11)$$

where a is the lattice constant (a = 2.98 Å in our case, assuming the hole transport is supported by Cu-planes[21]). The time τ_0 is defined by the approximation:

$$k_B T \cong \frac{h}{2\pi}\omega_0 \quad (12)$$

where $\omega_0 = \frac{2\pi}{\tau_0}$.

We obtained 1.5 × 10^{-12} s for τ and 1.6 × 10^{-13} s for τ_0, in our specific case. The condition (10) seems to be well respected, although the experimental confirmation of small polaron conductivity is often troubled by the effects of impurities, grain boundaries and temperature-dependent changes of the transport mechanism.[64,65] In our particular case, applying the small polaron model (Fig. 7(c)) leads to an activation energy of 81 meV, higher than 65 meV reported by Farrell *et al.*[49] using also a small polaron model. In our case, Hall mobility measurements at a high magnetic field and the corresponding calculation of the time for the hole transition from ion to ion suggest small polaron hopping (SPH) conductivity. However, one would definitely need further transport measurements like the Seebeck-coefficient as a function of temperature and complementary calculations based on corrected density functional theory to draw definitive conclusions if holes are lattice-bound in the room-temperature range.

For the very low temperature range of 30–90 K, none of the classical semiconductor or SPH models fits the experimental data. A variable range hopping (VRH) model is applied (Fig. 7(d)) as:[66,67]

$$\sigma = \sigma_0 e^{-\left(\frac{T_0}{T}\right)^{1/(n+1)}} \quad (13)$$

where σ_0 is a pre-exponential factor, T_0 is the Mott temperature and n is the dimension of the system. In our case, the best fit is obtained for n = 2 and T_0 = 79 K, suggesting that the hopping mechanisms of holes are confined to the two dimensions on the Cu-basal planes.

The electrical conductivity is mainly due to the high concentration of holes induced by crystalline point-defects. Considering the work reported by Ingram *et al.*[62] for $CuAlO_2$, a similar copper deficiency and an excess of +III cations (aluminium in their case) were noticed. p-Type conductivity was attributed to a complex defect of Al on a Cu-site stabilized by two bound oxygen interstitials $\left(Al_{Cu}^{\bullet\bullet} 2O_i''\right)''$. In our particular case, an excess of oxygen is not significantly detected and impairs to draw a similar conclusion that would imply the complexation of Cr with oxygen interstitials.[22] As an alternative hypothesis, we suggest that the excess of Cr *vs.* Cu is a specific feature for the growth of degenerated $CuCrO_2$ thin-films. Recent defect calculations on $CuCrO_2$ show that a copper vacancy is a shallow acceptor (0.37 eV) with the lowest intrinsic defect energy.[21] Additional defect energy calculations with an excess of Cr would provide critical insights to conclude on the results we are presenting in this paper. It is worth reminding that the electronegativity of Cu being considerably higher than that of Cr, a close-proximity of excess Cr in the interstitial site of O–Cu–O dumbbells would significantly impact the electronic configuration of Cu, in line with the observation of Cu^0 by XPS measurements.

Optical properties

The optical transmittance was measured in the range of 250–850 nm for films grown with $0.2 \leq \chi \leq 0.8$ at $T_{surface}$ = 370 °C, and the corresponding spectra are shown in Fig. 8(a). The range of thicknesses for all films is between 120 and 160 nm. The average transmittance in the 400–800 nm range decreases from 40–50%, for $0.2 \leq \chi \leq 0.6$, down to 30% for higher χ. For the latter case, the transmittance decrease is attributed to the concomitant existence of Cu_2O and CuO phases, having a much lower bandgap (2.2 eV[68,69] and 1.6 eV,[70,71] respectively) than $CuCrO_2$.

The pure phase delafossite features a higher averaged transmittance relative to the contaminated films with a maximum transparency for χ = 0.2. For this specific film, the transmittance improvement is mainly attributed to the morphology of the thin-film which is not continuous as evidenced by the SEM picture in Fig. 2(a).

The absorption coefficient α was calculated for various χ values using eqn (6). The absorption coefficient and the corresponding normalized derivative are plotted in Fig. 8(b). All films containing the delafossite phase show a steep increase of the absorption coefficient at 3.1–3.2 eV with the corresponding maximum for the derivative curve. This absorption is in line with the previously reported studies on the delafossite $CuCrO_2$ phase.[37,39,72,73] However, another steep increase of the absorption is noticed at 2.5 eV for $x \geq 0.66$. This absorption edge at 2.5 eV is particularly steep for the Cu_2O reference coating (χ = 1). This feature further confirms the growth of parasitic Cu_2O for $\chi \geq 0.66$.

The direct optical gap of $0.2 \leq \chi \leq 0.5$ is evaluated using a linear fit of Tauc's plot with the following relation:[74]

$$(\alpha h\nu)^2 = C(h\nu - E_g) \quad (14)$$

where $h\nu$ is the photon energy, C is a constant and E_g is the optical band gap. In our particular case, the use of standard Tauc's equation for degenerated semiconductors is an approximation. The extracted direct band gap E_g is found to be between 3.1 and 3.3 eV, which is in very good agreement with previous experimental and theoretical studies.[16,32,33,36,38,40,43,46,47]

The figure of merit (FOM) for a ratio of χ = 0.5 is calculated. FOM is defined as:

$$F = \frac{\sigma}{\alpha} \quad (15)$$

In order to compare the FOM with other groups, we assume for the FOM calculation that the absorption coefficient is expressed as:

$$\alpha = \frac{1}{d}\ln\left(\frac{1}{T_{av} + R_{av}}\right) \quad (16)$$

where T_{av} and R_{av} are transmittance and reflectance average in the visible range (400–800 nm).Then:

$$F = -\frac{1}{R_s \ln(T + R)} \quad (17)$$

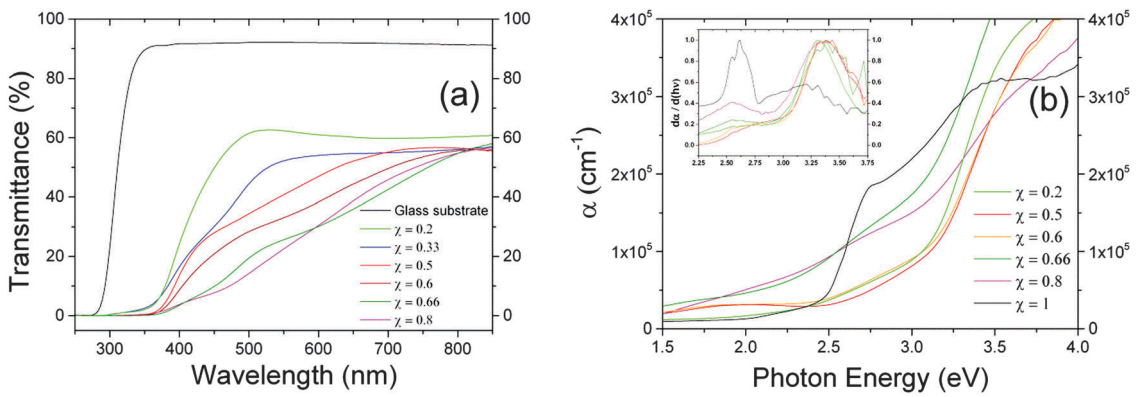

Fig. 8 (a) Transmittance spectra of films grown on glass substrates at $T_{surface}$ = 370 °C and for $0.2 \leq \chi \leq 0.8$. (b) Absorption coefficient for $0.2 \leq \chi \leq 1$ as a function of photon energy. The inset graph is the derivative of the absorption coefficient. Depositions were performed at 370 °C.

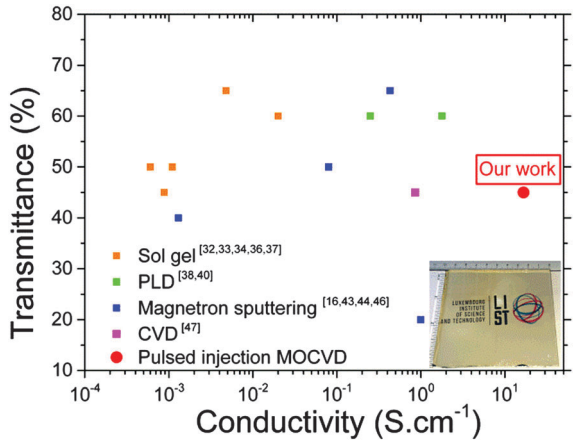

Fig. 9 Transmittance and conductivity reported in the literature for various syntheses. The inset picture shows CuCrO2 thin film deposited on a glass substrate with a 3.7 × 3.9 inch (9.3 × 9.8 cm) dimensions.

where R_s is the sheet resistance. We obtained a FOM of 2300 mS which is far higher than the best FOM recently reported (350 mS).[53]

When plotting the average transmittance (in the visible wavelength range), and the conductivity at room temperature that are obtained for thin films of $CuCrO_2$ grown by various synthesis methods, we compare the transparency/conductivity of our p-type thin films with reported data in the literature (Fig. 9). The thickness for all selected films is between 100 and 300 nm. It appears that the ''intrinsically doped'' thin-films that we grow using pulsed injection MOCVD show the best conductivity/transparency trade-off when compared to other synthesis methods. The picture in the inset shows that the MOCVD process is typically applied to a large surface area, 14.05 $inch^2$ in our case (91 cm^2) and can be up-scaled to larger glass or plastic substrates being resistant to temperature as high as 400 °C.

Conclusions

$CuCrO_2$ thin films were grown for the first time using the pulsed injection MOCVD process. A pure delafossite phase was obtained without any detectable carbon contamination. The substrate temperature and precursor mixing ratio are key factors in controlling the stoichiometry of the as-deposited films, for which an excess of Cr has been shown in single phase films. The value of 17 S cm^{-1} obtained for films deposited at 370 °C and with a precursor ratio $\chi = 0.5$ is the highest ever reported for ''undoped'' $CuCrO_2$ films while the corresponding band gap, 3.1–3.3 eV, enables a good optical transparency. These results definitely show again the interest of using $CuCrO_2$ thin-films that are grown using an up-scalable CVD process at low temperature (<400 °C) enabling the treatment of a very large glass surface. The growth of p-type transparent conducting oxides with excellent conductivity/transparency performances is reported and opens new avenues for the large scale fabrication of transparent electronic devices on glass. These original results show the potential of delafossite $CuCrO_2$ thin-films when considering the fabrication of transparent p-n junctions particularly suitable for electrical rectifying or photodetection purposes.

Acknowledgements

The authors would like to acknowledge Germain Rey and the financial support of the Fond National de la Recherche Luxembourg (FNR Luxembourg) through the INTER/MAT/11/02/PNOXIDES project.

References

1 G. Helwig, *Z. Phys.*, 1952, **132**, 621–642.
2 D. S. Ginley, H. Hosono and D. C. Paine, *Handbook of transparent conductors*, Springer, New York, 2010.
3 D. S. Ginley and C. Bright, *MRS Bull.*, 2000, **25**, 15–18.
4 F. Yang and S. R. Forrest, *Adv. Mater.*, 2006, **18**, 2018–2022.
5 Y. Z. Zheng, X. Tao, L. X. Wang, H. Xu, Q. Hou, W. L. Zhou and J. F. Chen, *Chem. Mater.*, 2010, **22**, 928–934.
6 J. Tate, M. K. Jayaraj, A. D. Draeseke, T. Ulbrich, A. W. Sleight, K. A. Vanaja, R. Nagarajan, J. F. Wager and R. L. Hoffman, *Thin Solid Films*, 2002, **411**, 119–124.
7 M. Gratzel, *Nature*, 1995, **414**, 338–344.
8 H. Hosono, *Int. J. Appl. Ceram. Technol.*, 2004, **1**, 106–118.
9 C. G. Granqvist and A. Hultåker, *Thin Solid Films*, 2002, **411**, 1–5.
10 M. Batzill and U. Diebold, *Prog. Surf. Sci.*, 2005, **79**, 47–154.
11 Ü. Özgür, Y. I. Alivov, C. Liu, A. Teke, M. A. Reshchikov, S. Do and V. Avrutin, *J. Appl. Phys.*, 2005, **98**, 041301.
12 H. Ohta, K. Kawamura, M. Orita, M. Hirano, N. Sarukura and H. Hosono, *Appl. Phys. Lett.*, 2000, **77**, 475–477.
13 M. A. Marquardt, N. A. Ashmore and D. P. Cann, *Thin Solid Films*, 2006, **496**, 146–156.
14 H. Kawazoe, M. Yasukawa, H. Hyodo, M. Kurita, H. Yanagi and H. Hosono, *Nature*, 1997, **389**, 939–942.
15 H. Kawazoe, H. Yanagi, K. Ueda and H. Hosono, *MRS Bull.*, 2000, **25**, 28–36.
16 R. Nagarajan, A. D. Draeseke, A. W. Sleight and J. Tate, *J. Appl. Phys.*, 2001, **89**, 8022–8025.
17 T. Arnold, D. J. Payne, A. Bourlange, J. P. Hu, R. G. Egdell, L. F. J. Piper, L. Colakerol, A. Masi, P. A. Glans, T. Learmonth, K. E. Smith, J. Guo, D. O. Scanlon, A. Walsh, B. J. Morgan and G. W. Watson, *Phys. Rev. B: Condens. Matter Mater. Phys.*, 2009, **79**, 075102.
18 D. O. Scanlon, A. Walsh, B. J. Morgan, G. W. Watson, D. J. Payne and R. G. Egdell, *Phys. Rev. B: Condens. Matter Mater. Phys.*, 2009, **79**, 035101.
19 D. O. Scanlon, K. G. Godinho, B. J. Morgan and G. W. Watson, *J. Chem. Phys*, 2010, **132**, 024707.
20 T. Yokobori, M. Okawa, K. Konishi, R. Takei, K. Katayama, S. Oozono, T. Shinmura, T. Okuda, H. Wadati, E. Sakai, K. Ono, H. Kumigashira, M. Oshima, T. Sugiyama, E. Ikenaga, N. Hamada and T. Saitoh, *Phys. Rev. B: Condens. Matter Mater. Phys.*, 2013, **87**, 195124.

21 D. O. Scanlon and G. W. Watson, *J. Mater. Chem.*, 2011, **21**, 3655.
22 D. O. Scanlon and G. W. Watson, *J. Phys. Chem. Lett.*, 2010, **1**, 3195–3199.
23 Y. Ono, K. I. Satoh, T. Nozaki and T. Kajitani, *Jpn. J. Appl. Phys.*, 2007, **46**, 1071–1075.
24 T. Okuda, N. Jufuku, S. Hidaka and N. Terada, *Phys. Rev. B: Condens. Matter Mater. Phys.*, 2005, **72**, 144403.
25 Y. Ma, X. Zhou, Q. Ma, A. Litke, P. Liu, Y. Zhang, C. Li and E. J. M. Hensen, *Catal. Lett.*, 2014, **144**, 1487–1493.
26 S. Kato, R. Kawashima and M. Ogasawara, *J. Mater. Sci.*, 2015, **50**, 2876–2883.
27 M. Amami, C. V. Colin, P. Strobel and A. Ben Salah, *Phys. B*, 2011, **406**, 2182–2185.
28 M. Poienar, F. Damay, C. Martin, V. Hardy, A. Maignan and G. André, *Phys. Rev. B: Condens. Matter Mater. Phys.*, 2009, **79**, 014412.
29 A. Maignan, C. Martin, R. Frésard, V. Eyert, E. Guilmeau, S. Hébert, M. Poienar and D. Pelloquin, *Solid State Commun.*, 2009, **149**, 962–967.
30 A. P. Amrute, Z. Łodziana, C. Mondelli, F. Krumeich and J. Pérez-Ramírez, *Chem. Mater.*, 2013, **25**, 4423–4435.
31 R. Bywalez, S. Götzendörfer and P. Löbmann, *J. Mater. Chem.*, 2010, **20**, 6562–6570.
32 M. Han, K. Jiang, J. Zhang, W. Yu, Y. Li, Z. Hu and J. Chu, *J. Mater. Chem.*, 2012, **22**, 18463–18470.
33 M. J. Han, Z. H. Duan, J. Z. Zhang, S. Zhang, Y. W. Li, Z. G. Hu and J. H. Chu, *J. Appl. Phys.*, 2013, **114**, 163526.
34 H.-Y. Chen and K.-P. Chang, *ECS J. Solid State Sci. Technol.*, 2013, **2**, P76–P80.
35 M. Asemi and M. Ghanaatshoar, *J. Sol-Gel Sci. Technol.*, 2014, **70**, 416–421.
36 J. Wang, P. Zheng, D. Li, Z. Deng, W. Dong, R. Tao and X. Fang, *J. Alloys Compd.*, 2011, **509**, 5715–5719.
37 H.-Y. Chen, K.-P. Chang and C.-C. Yang, *Appl. Surf. Sci.*, 2013, **273**, 324–329.
38 D. Li, X. Fang, Z. Deng, S. Zhou, R. Tao, W. Dong, T. Wang, Y. Zhao, G. Meng and X. Zhu, *J. Phys. D: Appl. Phys.*, 2007, **40**, 4910–4915.
39 P. W. Sadik, M. Ivill, V. Craciun and D. P. Norton, *Thin Solid Films*, 2009, **517**, 3211–3215.
40 F. Lin, C. Gao, X. Zhou, W. Shi and A. Liu, *J. Alloys Compd.*, 2013, **581**, 502–507.
41 K. Tonooka and N. Kikuchi, *Thin Solid Films*, 2006, **515**, 2415–2418.
42 D. Li, X. Fang, A. Zhao, Z. Deng, W. Dong and R. Tao, *Vacuum*, 2010, **84**, 851–856.
43 R.-S. Yu and C.-P. Tasi, *Ceram. Int.*, 2014, **40**, 8211–8217.
44 H. Sun, M. Arab Pour Yazdi, P. Briois, J.-F. Pierson, F. Sanchette and A. Billard, *Vacuum*, 2015, **114**, 101–107.
45 T.-W. Chiu, Y.-C. Yang, A.-C. Yeh, Y.-P. Wang and Y.-W. Feng, *Vacuum*, 2013, **87**, 174–177.
46 G. Dong, M. Zhang, X. Zhao, H. Yan, C. Tian and Y. Ren, *Appl. Surf. Sci.*, 2010, **256**, 4121–4124.
47 S. Mahapatra and S. A. Shivashankar, *Chem. Vap. Deposition*, 2003, **9**, 238–240.
48 S. H. Lim, S. Desu and A. C. Rastogi, *J. Phys. Chem. Solids*, 2008, **69**, 2047–2056.
49 L. Farrell, E. Norton, B. J. O. Dowd, D. Caffrey, I. V Shvets and K. Fleischer, *Appl. Phys. Lett.*, 2015, **107**, 031901.
50 T. S. Tripathi, J.-P. Niemelä and M. Karppinen, *J. Mater. Chem. C*, 2015, **3**, 8364–8371.
51 A. C. Rastogi, S. H. Lim and S. B. Desu, *J. Appl. Phys.*, 2008, **104**, 023712.
52 J. Crêpellière, N. Bahlawane, S. Siebentritt and D. Lenoble, in *5th International Symposium on Transparent Conductive Materials*, Chania, Crete, 2014.
53 L. Farrell, E. Norton, C. M. Smith, D. Caffrey, I. Shvets and K. Fleischer, *J. Mater. Chem. C*, 2015, **4**, 126–134.
54 J. Pankove, *Optical Processes in Semiconductors*, Dover Publication, New York, 1971.
55 W. Dannhauser and P. A. Vaughan, *J. Am. Chem. Soc.*, 1955, **77**, 896.
56 O. Crottaz and F. Kubel, *Z. Kristallogr.*, 1996, **211**, 482.
57 C. D. Wagner, W. M. Riggis, L. E. Davis, J. F. Moulder and G. E. Mulenberg, *Handbook of X-Ray Photoelectron Spectroscopy*, Perkin Elmer, Minnesota, 1979.
58 N. Pauly, S. Tougaard and F. Yubero, *Surf. Sci.*, 2014, **620**, 17–22.
59 M. O'Sullivan, P. Stamenov, J. Alaria, M. Venkatesan and J. M. D. Coey, *J. Phys.: Conf. Ser.*, 2010, **200**, 052021.
60 A. Barnabé, Y. Thimont, M. Lalanne, L. Presmanes and P. Tailhades, *J. Mater. Chem. C*, 2015, **3**, 6012–6024.
61 N. W. Ashcroft and N. D. Mermin, *Solid State Physics*, Holt, New York, 1976.
62 B. J. Ingram, G. B. Gonzalez, T. O. Mason, D. Y. Shahriari, A. Barnabe, D. Ko and K. R. Poeppelmeier, *Chem. Mater.*, 2004, **16**, 5616–5622.
63 B. J. Ingram, B. J. Harder, N. W. Hrabe, T. O. Mason and K. R. Poeppelmeier, *Chem. Mater.*, 2004, **16**, 5623–5629.
64 A. J. Bosman and H. J. van Daal, *Adv. Phys.*, 1970, **19**, 1–117.
65 A. R. Nagaraja, N. H. Perry, T. O. Mason, Y. Tang, M. Grayson, T. R. Paudel, S. Lany and A. Zunger, *J. Am. Ceram. Soc.*, 2012, **95**, 269–274.
66 N. F. Mott, *J. Non-Cryst. Solids*, 1968, **1**, 1–17.
67 N. F. Mott, *Philos. Mag.*, 1969, **19**, 835–852.
68 B. K. Meyer, A. Polity, D. Reppin, M. Becker, P. Hering, P. J. Klar, T. Sander, C. Reindl, J. Benz, M. Eickhoff, C. Heiliger, M. Heinemann, J. Bläsing, A. Krost, S. Shokovets, C. Müller and C. Ronning, *Phys. Status Solidi B*, 2012, **249**, 1487–1509.
69 C. Malerba, F. Biccari, C. Leonor Azanza Ricardo, M. D'Incau, P. Scardi and A. Mittiga, *Sol. Energy Mater. Sol. Cells*, 2011, **95**, 2848–2854.
70 B. V. Karpenko, a. V. Kuznetsov and V. V. Dyakin, *J. Phys.: Condens. Matter*, 1996, **8**, 1785–1795.
71 F. G. Marabelli, B. Parravicini and F. Salghetti-Drioli, *Phys. Rev. B: Condens. Matter Mater. Phys.*, 1995, **52**, 1433–1436.
72 H. Hiraga, T. Makino, T. Fukumura, H. Weng and M. Kawasaki, *Phys. Rev. B: Condens. Matter Mater. Phys.*, 2011, **84**, 041411(R).
73 D. Shin, J. S. Foord, R. G. Egdell and A. Walsh, *J. Appl. Phys.*, 2012, **112**, 113718.
74 P. Y. Yu and M. Cardona, *Fundamentals of Semiconductors*, Springer, Berlin, 2005.

